JOM, Vol. 71, No. 2, 2019
https://doi.org/10.1007/s11837-018-3203-7
© 2018 The Minerals, Metals & Materials Society

Characterization of Cavity Oscillation and Splashing Distribution Under Excitation by Bottom Gas Blowing in a Steelmaking Converter

MINGMING LI,[1,2] QIANG LI,[1] ZONGSHU ZOU,[1] and BAOKUAN LI[1]

1.—School of Metallurgy, Northeastern University, P.O. Box 312, 3-11 Wenhua Road, Heping District, Shenyang 110819, People's Republic of China. 2.—e-mail: limm@smm.neu.edu.cn

The cavity oscillation and splash characteristics dominate the operational stability and refining efficiency in converter steelmaking processes. These characteristics under excitation by bottom gas blowing in a steelmaking converter were evaluated using a developed filter-based multifluid model. The cavity oscillation mechanism was examined by reference to cavity surface flows, and its characteristics were quantified in terms of frequency and amplitude using the fast Fourier transform approach. The splashing distribution describing the splashing droplet size and rate under various operating conditions was clarified. The results reveal that the cavity oscillation and splashing distribution are mainly controlled by the cavity surface flow velocity, which itself is influenced by the operating conditions. Use of bottom gas blowing intensifies the cavity oscillation in terms of both frequency and amplitude, and increases the splashing rate, but decreases the droplet size by accelerating the cavity surface flow. The lance height plays a dominant role in forming the cavity oscillation and controlling the splashing distribution.

INTRODUCTION

Cavity oscillation and bath splashing are important physical phenomena in oxygen converter steelmaking processes, dominating the refining efficiency and operational stability to a certain extent. It has been acknowledged that bath splashing and spitting originate from the cavity and are strongly related to its oscillatory movement.[1–3] Additionally, the oscillating cavity provides a stimulus for formation of bath surface waves, which profoundly influence not only the behavior of the bath, e.g., the splashing distribution, but also the localized wear of the furnace wall.[4,5] As such, insight into the characteristics of the cavity oscillation and the related bath splashing behavior can provide an important foundation for understanding and improving converter performance.

In previous study,[6] the frequency of the cavity oscillation was reported to lie between 5 Hz and 16 Hz for pure top-blown converters. Sabah and Brooks[2] quantified the amplitude and frequency of the cavity oscillation using the fast Fourier transform (FFT) technique in an air–water model that simulates a pure top-blown converter system, reporting an overall frequency range from 3 Hz to 9 Hz, depending on the cavity modes, which were themselves determined by the blowing parameters and corresponded to different splashing distributions. In modern converter steelmaking, inert gas is additionally injected from the bottom of the furnace in the form of bubbling plumes. These bubbling plumes inevitably interact with the cavity, and are expected to modify the cavity oscillation behavior and bath splashing distribution.[7–9] Fabritius et al.[10,11] and Odenthal et al.[12] showed based on physical and numerical experiments, respectively, that the bubbling plumes from submerged side-blown nozzles in argon oxygen decarburization converters induced oscillation of the entire bath. Although extensive attention has already been paid to cavity oscillation and bath splashing, there is still a lack of quantitative evaluation on how bottom gas blowing influences the cavity oscillation behavior and splashing distribution in combined-blown converter steelmaking processes. Therefore, in this work, characterization of the cavity oscillation and bath splashing distribution under excitation by

(Published online November 1, 2018)

bottom gas blowing in a combined-blown converter was performed, using a developed multifluid model combining the volume of fluid (VOF) approach and discrete particle model (DPM) with a filtered turbulence method. The results of the developed model reveal the mechanism of cavity oscillation generation and quantify the oscillation characteristics as well as splashing distribution, enabling comprehensive evaluation of the influence of the blowing parameters.

MATHEMATICAL MODEL

The combined-blown converter steelmaking process, which features supersonic oxygen jets impinging on the molten bath with inert gas blowing from the bottom of the furnace, was simulated based on the unsteady Reynolds-averaged Navier–Stokes equations, closed using a filtered k–ε turbulence model,[13] where the turbulent viscosity μ_t was modeled using a filter with the scaling function defined in Eq. 1.

$$\mu_t = f \cdot \mu_{t,\mathrm{std}} = \min\left[1, C_3 \Delta \frac{\varepsilon}{k^{3/2}}\right] \mu_{t,\mathrm{std}} \tag{1}$$

where $\mu_{t,\mathrm{std}}$ is the turbulent viscosity defined in the standard k–ε model, C_3 is a constant equal to 1, f is termed the blending function and helps to ensure that the wall functions work at near-wall nodes by returning a value of 1, and Δ is termed the filter size, used to separate smaller-scale turbulent eddies from larger ones. In this turbulence model, the smaller-scale eddies are modeled while larger-scale ones are resolved directly. To ensure that the numerically resolvable scale is compatible with the filtering process, the following condition should be satisfied:

$$\Delta = \max\left[\Delta_{\mathrm{present}}, \Delta_{\mathrm{grid}}\right] \tag{2}$$

where $\Delta_{\mathrm{grid}} = (\Delta x \cdot \Delta y \cdot \Delta z)^{1/3}$. In this study, the filter size was defined as varying in space, depending on the local grid size. This turbulence model is based on the local meshing resolution and was confirmed to be superior for the description of turbulent flows inside the bath in our previous study.[14] The VOF model[15] was used to simulate the transient features of the top jets impinging on the bath surface and to track the deformed gas–liquid interface. In this model, a single set of momentum equations is shared by both the liquid and gas phase, being solved to determine the phase-shared field variables. The effect of surface tension was addressed using a continuum surface force model [16] in which the surface tension is considered to be a continuous force across the interface.

The trajectories of the bubbles of gas blown in from the bottom of the furnace were calculated using the DPM,[17] where each bubble was tracked by solving Newton's second law, integrating the drag, gravitational, virtual mass, and pressure gradient forces. The possible effect of irregular bubble shapes arising inside the bath due to their motion was introduced by a user-defined function (UDF) to modify the drag coefficient C_D according to the relative Reynolds number range[18] as follows:

$$C_D = \begin{cases} 16/\mathrm{Re} & \mathrm{Re} \le 1.5 \\ 14.9\mathrm{Re}^{-0.78} & 1.5 < \mathrm{Re} \le 80 \\ 48/\mathrm{Re}(1 - 2.21\mathrm{Re}^{-0.5}) & 80 < \mathrm{Re} \le 700 \\ 1.86 \times 10^{-15}\mathrm{Re}^{4.756} & 700 < \mathrm{Re} \le 1530 \\ 2.61 & 1530 < \mathrm{Re} \end{cases} \tag{3}$$

The injection of gas at the bottom of the furnace was realized using a uniform bubble distribution with initial bubble diameter of d_0, as shown in Eq. 4.[19] The bubble size varies with the local pressure as the bubble rises, which was included using another UDF as defined in Eq. 5. Meanwhile, another UDF was defined to cease tracking bubbles that reached the gas–liquid interface.

$$d_0 = \left\{ \left(\frac{\sigma d_{\mathrm{tuy}}}{\rho_l g}\right)^2 + 0.03325 \left[\left(\frac{Q_B}{N_B}\right)^2 d_{\mathrm{tuy}}\right]^{0.867} \right\}^{0.167} \tag{4}$$

$$d = d_0\left(1 + \frac{\rho_1 g h}{p}\right)^{\frac{1}{3}} \tag{5}$$

where σ is the surface tension of liquid phase, ρ_1 is the liquid density, d_{tuy} is the bottom tuyere diameter, Q_B is the bottom gas flow rate, and N_B is the number of bottom tuyeres. The initial rising velocity of a bubble u_0 is expressed as follows[19]:

$$u_0 = \left(\frac{2\sigma}{\rho d_0} + 0.5 g d_0\right)^{0.5} \tag{6}$$

In principle, the flows of the bubbling plumes and the continuous phase are two-way coupled; i.e., the turbulent flow of the continuous phase influences the trajectories of the bubbles, and in turn the presence of the dispersed phase affects the turbulence in the continuous phase. Consequently, a random walk model[17] was used to account for the "stochastic" effect of turbulent fluctuations on the motion of the bubbles. In this model, the fluctuation in the bubble velocity was estimated by a Gaussian-distributed random number chosen according to the local turbulence kinetic energy. A new instantaneous velocity fluctuation is produced by changing the random number at a frequency equal to the characteristic lifetime of the turbulent eddy. The instantaneous fluid velocity is then given by

$$\boldsymbol{u} = \bar{\boldsymbol{u}} + \boldsymbol{u}' \tag{7}$$

$$\boldsymbol{u}' = \xi\sqrt{\overline{\boldsymbol{u}'^2}} = \xi\sqrt{\frac{2k}{3}} \tag{8}$$

where $\bar{\boldsymbol{u}}$ the mean liquid velocity, $\boldsymbol{u}'$ is the random fluctuating liquid velocity, ξ is a normally distributed random number, and k is the local turbulent kinetic energy.

Simulations were carried out by scaling a 125-t converter down to 1:6. The gas–metal system in the absence of slag was considered, represented by an air–water system. The arrangements of the top lance nozzles and bottom tuyeres are shown in Fig. 1. In this model, the top lance is equipped with six nozzles having outlet diameter of 8.6 mm and throat diameter of 6.3 mm. The lance height was varied from 0.2 m to 0.3 m. The top and bottom gas flow rates were also varied in the simulations, in the range of 117.3 Nm^3/h to 135.9 Nm^3/h and of 0.79 Nm^3/h to 1.95 Nm^3/h, respectively. As such, the top gas jet velocity at the nozzle outlet lay in the range from 111.8 m/s to 130.0 m/s. To improve the computational efficiency, the converter domain was reduced and only its lower part was modeled, as shown schematically in Fig. 1. In this reduced model, a profile data interpolation method [20] was employed for the inlet boundary where the velocity boundary condition was defined, as detailed elsewhere.[14] Meanwhile, a pressure boundary condition was used at the outlet and no-slip boundary conditions with a standard wall function were used at the wall, off which bubbles were allowed to reflect. A geometric reconstruction scheme was used to track the deformation of the free surface induced by the top gas impinging jets. Pressure–velocity decoupling was achieved using the pressure implicit split operator (PISO) algorithm, while the pressure staggering option (PRESTO) scheme was employed to interpolate the pressure values at the cell faces from the surrounding cell nodes in the solution of the momentum equations. A second-order upwind scheme was applied to discretize the convection terms of the momentum and turbulence conservative equations. The simulations were carried out using the ANSYS-Fluent platform with embedded user-defined subroutines. The convergence criterion was for the normalized residuals of all variables to be less than 1×10^{-4}.

This mathematical model was validated by comparing the numerical results with water model experimental data with respect to the cavity depth and bath mixing time. The details were described in our previous study[14] and thus are not presented here. Overall, reasonably good agreement between the simulated and measured results was achieved.

RESULTS AND DISCUSSION

Cavity Surface Flow

Figure 2 shows the time-averaged velocity distribution on the bath surface for the top and top–bottom combined blowing processes. It can be observed that, in general, the combined blowing process exhibits a higher flow velocity on the cavity surface and even over the entire bath surface in comparison with the top blowing process. The maximum cavity surface velocity increases from 0.65 m/s to 0.90 m/s when the blowing mode is changed from top to combined blowing with bottom gas flow rate of 1.22 Nm^3/h. Previous studies [1–3,5] have shown that the flows across the cavity surface make the cavity invariably astatic. The astatic cavity is accompanied simultaneously by surface waves that arise from the Kelvin–Helmholtz instability and propagate across the entire bath surface. Accordingly, the cavity moves time-dependently in

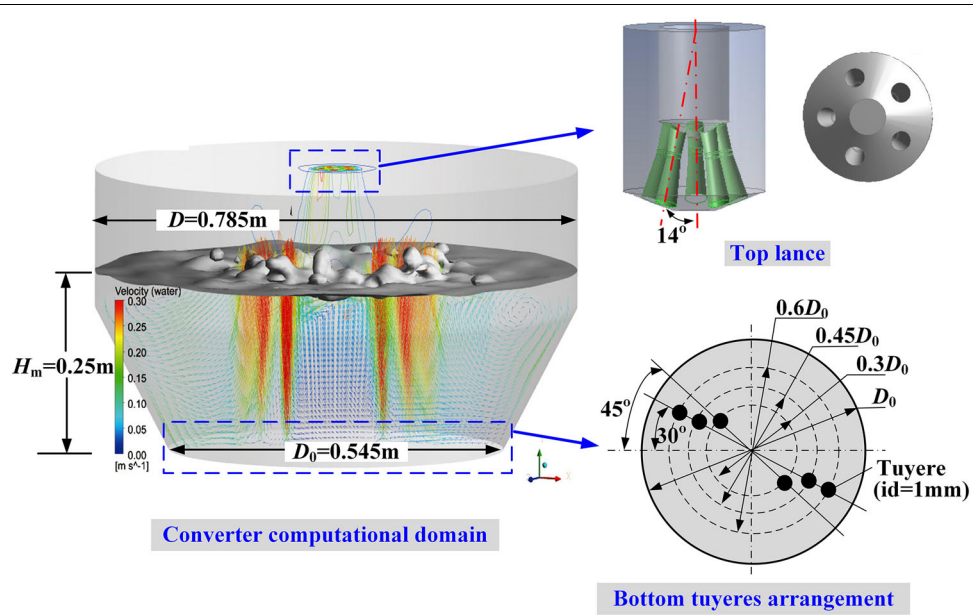

Fig. 1. Schematic diagram of converter computational domain.

both the up–down and right–left directions, exhibiting oscillatory movement. Higher cavity surface velocity is believed to intensify such cavity oscillation. The simulation results indeed show that the cavity oscillates more intensively in the combined-blown converter compared with the top-blown converter.

Cavity Oscillation Characteristics

To quantify the cavity oscillation, the instantaneous cavity depth was monitored by setting a line at the central axis of the furnace, as shown in Fig. 3a. The cavity depth is thus calculated as follows:

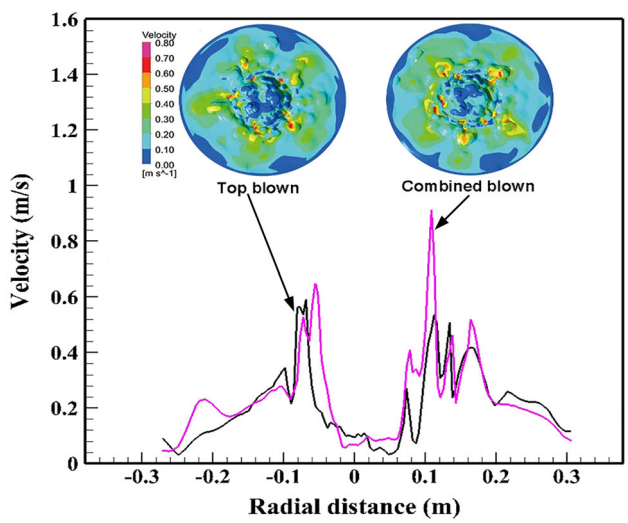

Fig. 2. Velocity distribution on the bath surface for top and combined blowing processes.

$$H_c = H_m\left(1 - \frac{\alpha_t(\text{water})}{\alpha_0(\text{water})}\right) \tag{9}$$

where H_c is the cavity depth, and α_t(water) and α_0(water) are the vertex-averaged water volume fraction on the monitoring line, at the any blowing moment and the initial time, respectively. The cavity depth recorded as a function of blowing time is shown in Fig. 3b, c. The results indicate that the cavity in the combined-blown converter is more unstable and requires a longer time to reach a quasistable state, while the cavity depth is hardly affected by the blowing mode.

Using the FFT technique[21] on the recorded time series of cavity depth, the representative frequency and amplitude of the cavity oscillation for both blowing modes are plotted in Fig. 4. It can be seen that there are a number of frequencies present, the highest for top and combined blowing being 11.7 Hz and 21.1 Hz, respectively. A dominant frequency (4 Hz) with the highest amplitude of 0.0012 m is present for combined blowing, but not for top blowing. It is worth noting that Sabah[2] and Peaslee[6] respectively reported that, for top blowing, the frequency ranges were 3 Hz to 9 Hz and 5 Hz to 16 Hz, and they likewise found that there was no one dominant frequency with highest amplitude. The present simulation results are compatible with the reported ones. Besides, it is found that the highest amplitude increases from 0.7 mm to 1.2 mm when the blowing mode was changed from top to combined blowing. These results confirm that bottom gas blowing indeed intensifies the cavity oscillation in terms of both frequency and amplitude.

In converter steelmaking processes, both the frequency and amplitude of the cavity oscillation represent the energy of the wave that forms and spreads out on the cavity surface, driving the bath surface flow. This wave movement is responsible for

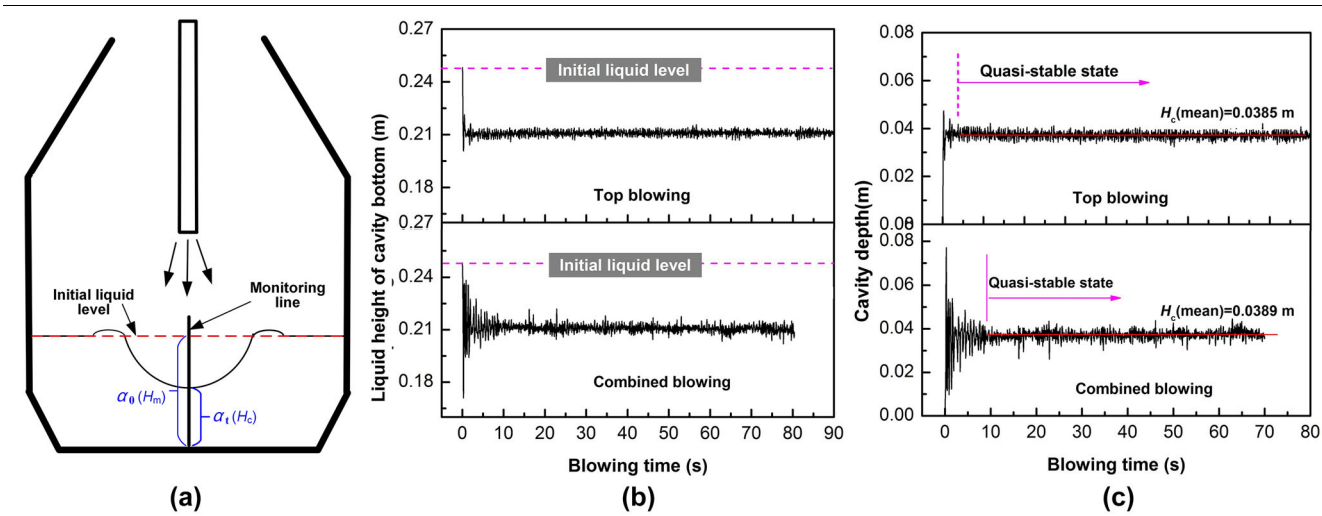

Fig. 3. (a) Determination of the cavity depth, (b) recorded liquid level height at cavity bottom, and (c) cavity depth versus blowing time for the top and combined blowing modes.

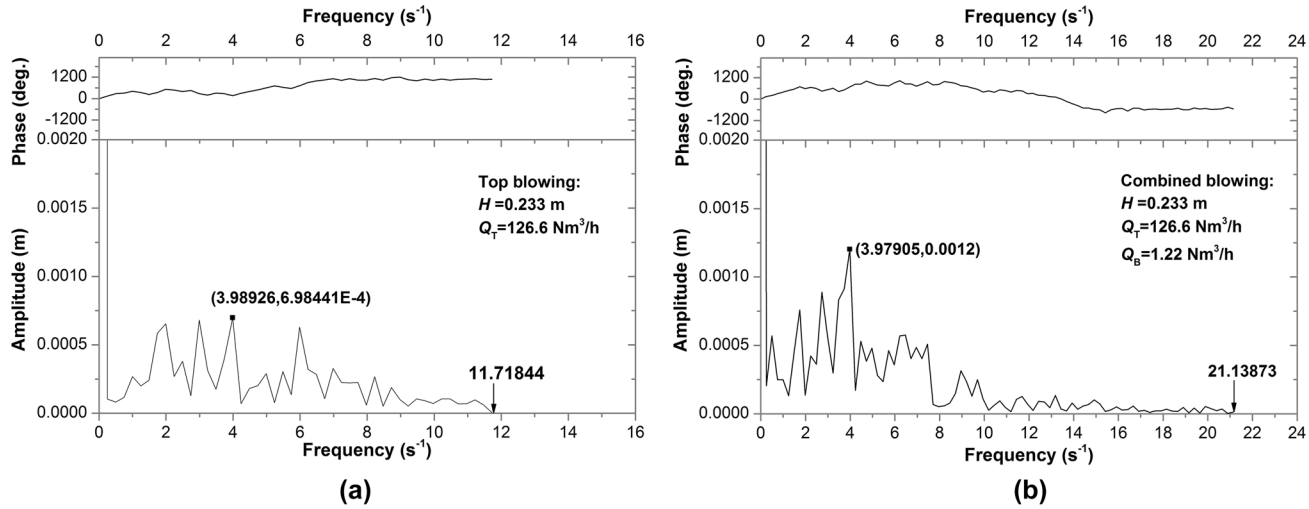

Fig. 4. FFT of time series of cavity depth for (a) top blowing, and (b) combined blowing.

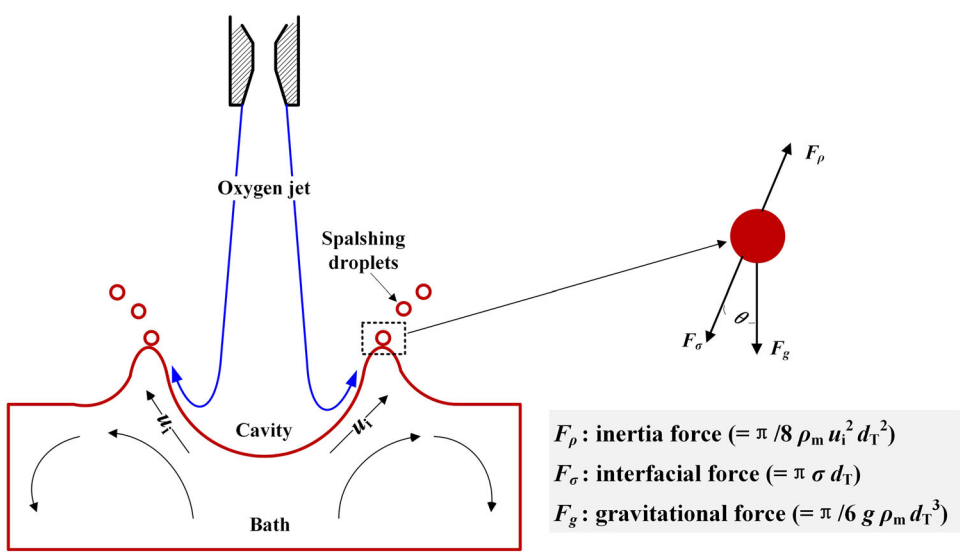

Fig. 5. Schematic diagram of generation of splashing droplets in steelmaking converters.

localized wear on the furnace wall and generation of splashing. According to fluid mechanics, a wave with higher frequency and/or amplitude, on the one hand, causes the energetic melt to wipe up and down the furnace wall more frequently and over a great range, and on the other hand provides greater energy to tear metal from the bath bulk. In this sense, in the combined-blown converter, the wall wear will be more serious, and splashing will be increased in comparison with the top-blown converter.

Splashing Distribution

In oxygen converter steelmaking processes, high-speed gas jets impinge on the molten bath surface and break metal off from the main liquid bath, creating metal droplets. A representative droplet generation according to this effect is shown schematically in Fig. 5. According to Oeters' theory,[22] a droplet at its detachment point is subject to inertial (F_ρ), interfacial (F_σ), and gravitational forces (F_g), as shown in Fig. 5. The condition for generation of a droplet can thus be expressed using Eq. 10. As such, the critical cavity surface flow velocity ($u_{i,\mathrm{crit}}$) for droplet generation, the actual droplet diameter (d_T), and the droplet generation rate (m_T) are as follows:

$$F_\rho \geq F_\sigma + F_g \cos\theta \tag{10}$$

$$u_{i,\mathrm{crit}} = \left(\frac{8}{\rho_\mathrm{m}}\right)^{1/2} \left(\frac{2}{3}\sigma g \rho_\mathrm{m} \cos\theta\right)^{1/4} \tag{11}$$

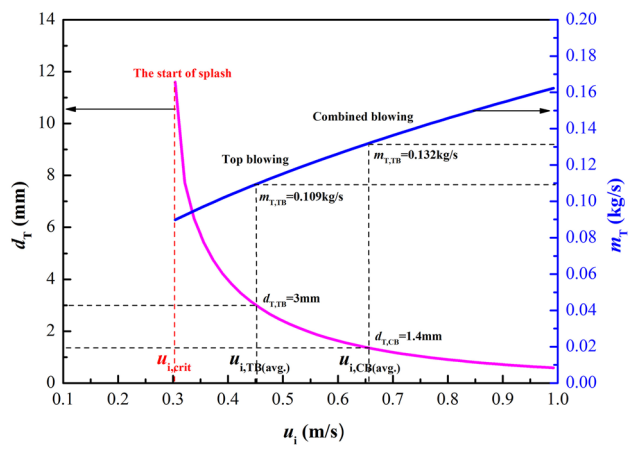

Fig. 6. Diameter and generation rate of splashing droplets as functions of cavity surface flow velocity under blowing conditions with lance height of 0.233 m, top gas flow rate of 126.6 Nm^3/h, and bottom gas flow rate of 1.22 Nm^3/h.

$$d_T = \frac{3}{8}\frac{u_i^2}{g\cos\theta}\left[1-\left(1-\frac{128\sigma g\cos\theta}{3\rho_m u_i^4}\right)^{\frac{1}{2}}\right] \quad (12)$$

$$m_T = \frac{1}{6}\pi\, d_T^3\rho_m \frac{0.4153D\rho_m^{1/2}\eta_m^{1/2}l_m^{1/2}u_i^{5/2}}{d_T^2\sigma+\frac{1}{6}d_T^4\rho_m g\cos\theta} \quad (13)$$

where ρ_m is the liquid density, σ is the interfacial tension, D is the cavity diameter, η_m is the viscosity, and l_m is the flow through the length of the droplet.

Figure 6 plots the diameter of splashing droplets and their generation rate as a function of the cavity surface flow velocity under representative blowing conditions (lance height of 0.233 m, top gas flow rate of 126.6 Nm^3/h, and bottom gas flow rate of 1.22 Nm^3/h). Based on these simulation results, the cavity depth and diameter are 0.039 m and 0.266 m, respectively, hence the value of cos θ is 0.281 under such conditions. According to Eq. 11, the critical cavity surface flow velocity for droplet generation is thus determined to be 0.304 m/s. It is of interest to note from this figure that the diameter of the splashing droplets decreases sharply with increase of the cavity surface flow velocity, while the generation rate of splashing droplets increases gradually. Furthermore, it is observed that the average droplet diameter is 3 mm and 1.4 mm and the average droplet generation rate is 0.109 kg/s and 0.132 kg/s, for the top and combined blowing mode, respectively. These results show that, compared with the top-blown converter, the more energetic cavity surface wave in the combined-blown converter principally contributes to the generation of smaller but many more droplets, which helps to form a more highly dispersed foam slag. It should be pointed out that such a splashing distribution is obtained by taking a time–space average over the cavity surface flow velocity. However, both the splashing droplet diameter and generation rate in fact exhibit irregular time–space distributions due to the transient behavior of the blowing processes.

Effects of Operating Parameters

To evaluate the effects of variation of the operating parameters on the cavity oscillation behavior, the highest amplitude and frequency of the cavity oscillation are considered. Figure 7a–c shows the highest frequency of the cavity oscillation for different lance heights, and top and bottom gas flow rates, respectively. In summary, the highest frequency increases with decrease in the lance height or increase of the top gas flow rate, but is independent of the bottom gas flow rate. Specifically, the highest frequency decreases from 27.8 Hz to 12.5 Hz as the lance height is increased from 0.2 m to 0.3 m. On the other hand, it increases from 17.9 Hz to 24.2 Hz as the top gas flow rate is increased from 117.3 Nm^3/h to 135.9 Nm^3/h. The effect of these operating parameters on the highest amplitude of the cavity oscillation is shown in Fig. 7d–f. It can be observed that the highest amplitude, with a range of 0.55 mm to 1.45 mm, increases with decrease of the lance height, but increase of the top or bottom gas flow rate. Notably, the lance height in the combined-blown converter steelmaking process seems to play a dominant role in the generation of the cavity oscillation, and as a result in causing splashing and thus wear of the refractory wall lining.

Figure 8 shows the effects of the operating parameters on the splashing distribution, revealing that the splashing droplet diameter decreases with decrease of the lance height, or increase of the top and bottom gas flow rate, owing to the enhanced cavity surface flow, while the generation rate of splashing droplets exhibits the opposite trend. These results further confirm that, as mentioned above, the lance height has a more significant influence on the splashing distribution in combined-blown converter steelmaking processes.

CONCLUSIONS

The cavity oscillation and splashing distribution with excitation by bottom gas blowing in a combined-blown steelmaking converter were characterized using a numerical model in combination with a theoretical model. The findings of the present study can be summarized as follows:

(1) The cavity oscillation is dominated by the cavity surface flow, which is intensified by the introduction of bottom gas blowing. Both the highest frequency and amplitude of the cavity oscillation thus increase when the top blowing mode changes to the top–bottom combined blowing mode. The highest frequency of the cavity oscillation for the present combined-

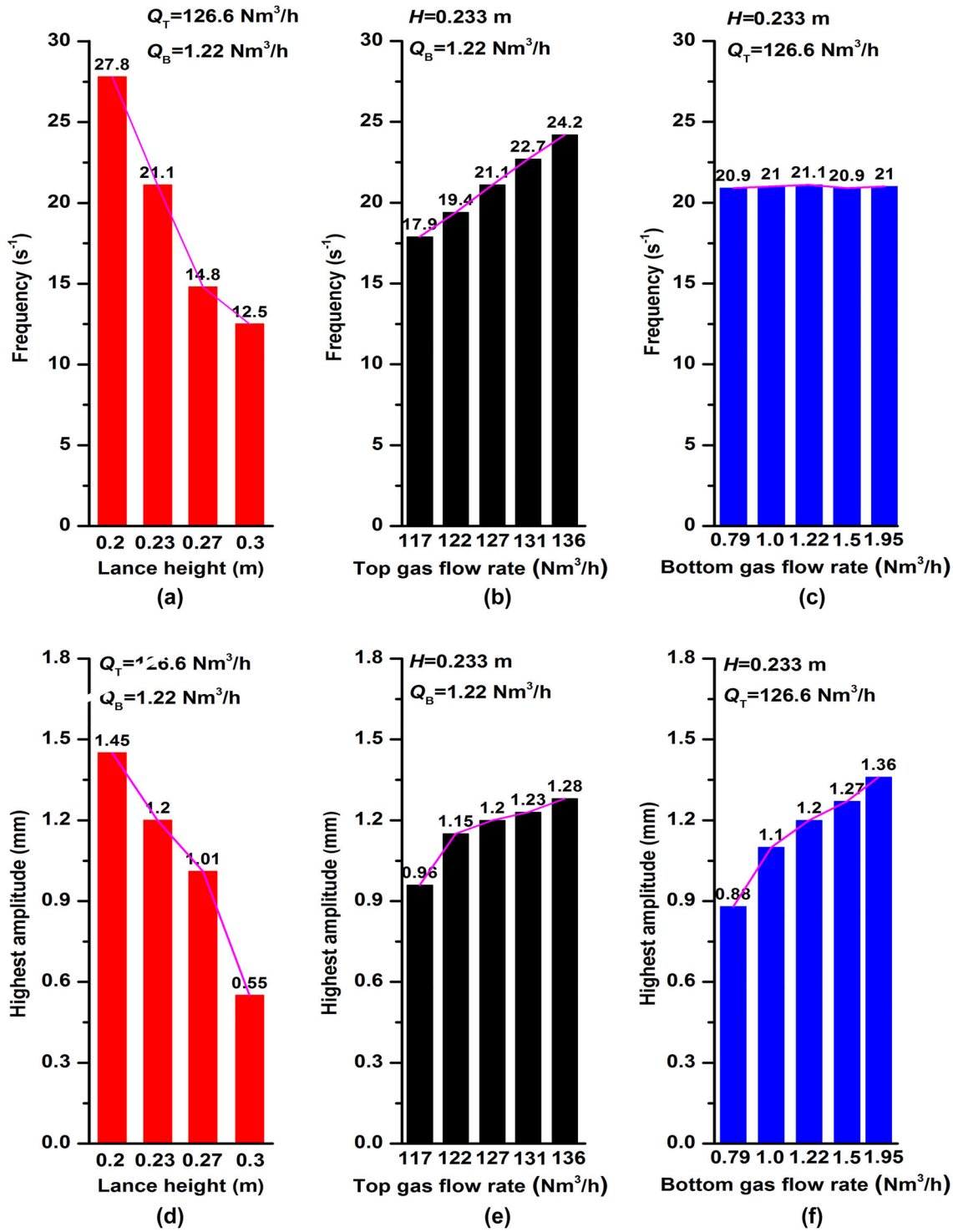

Fig. 7. Highest frequency of cavity oscillation for different operating parameters with respect to (a) lance height, (b) top gas flow rate, and (c) bottom gas flow rate, and highest amplitude of cavity oscillation at different (d) lance heights, (e) top gas flow rates, and (f) bottom gas flow rates.

blown converter lies in the range of 17.9–24.2 Hz.

(2) The highest frequency and amplitude of the cavity oscillation generally increase when decreasing the lance height or increasing the top and bottom gas flow rate, whereas the highest frequency is independent of the bottom gas flow rate. The lance height plays a dominant role in the generation of the cavity oscillation.

(3) The splashing characteristics are mainly controlled by the cavity surface flow. The top–bottom combined blowing mode contributes to increase the splashing rate but decreases the

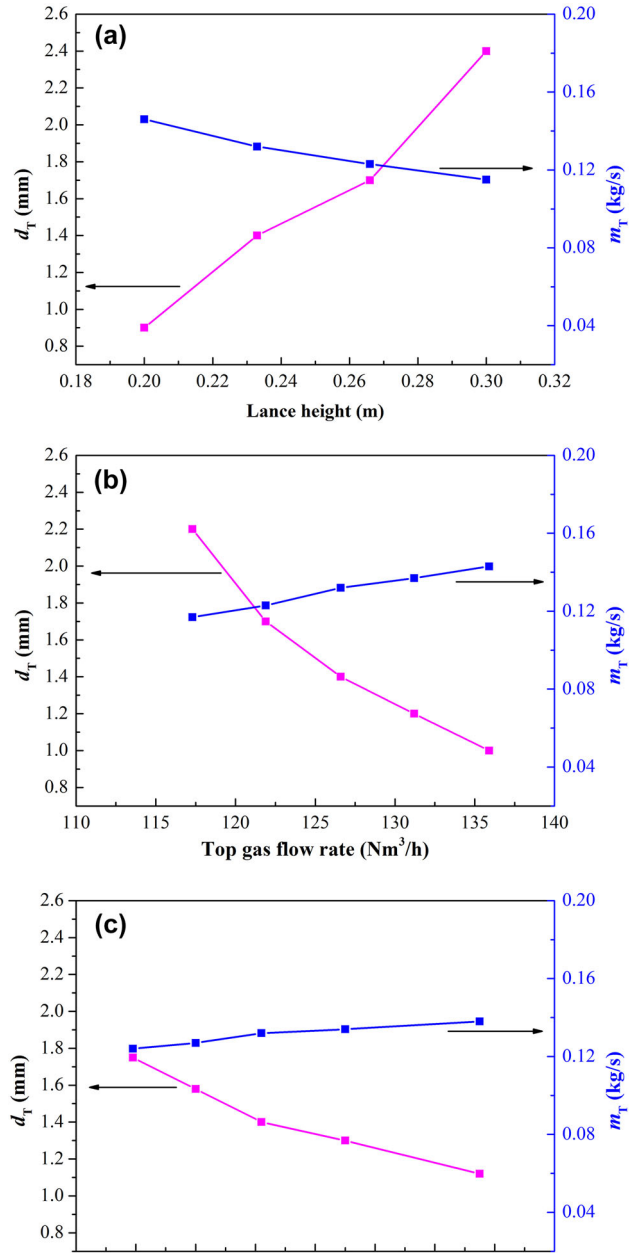

Fig. 8. Effects of operating parameters on the splashing distribution: (a) lance height, (b) top gas flow rate, and (c) bottom gas flow rate.

size of the splashing droplets in comparison with the pure top blowing mode. The droplet diameter decreases with decrease of the lance height, or increase of the top and bottom gas flow rate, whereas the splashing rate exhibits the opposite trend. The lance height has a more significant influence on the splashing distribution compared with other operating parameters.

ACKNOWLEDGEMENT

The authors are grateful for financial support from the Fundamental Research Funds for the Central Universities of China (N172503014).

REFERENCES

1. H.Y. Hwang and G.A. Irons, *Metall. Mater. Trans. B* 42, 575 (2011).
2. S. Sabah and G. Brooks, *ISIJ Int.* 54, 836 (2014).
3. M.M. Li, Q. Li, S.B. Kuang, and Z.S. Zou, *Ind. Eng. Chem. Res.* 55, 3630 (2016).
4. M. Lee, S.L. O'Rourke, and N. Molloy, *Scand. J. Metall.* 32, 281 (2003).
5. Q. Li, M.M. Li, S.B. Kuang, and Z.S. Zou, *JOM* 68, 3126 (2018).
6. K.D. Peaslee and D.G.C. Robertson, *EPD Congress, TMS* (PA: Warrendale, 1994).
7. N. Standish and Q.L. He, *ISIJ Int.* 29, 455 (1989).
8. M.J. Luomala, T.M.J. Fabiritius, and J.J. Härkki, *ISIJ Int.* 44, 809 (2004).
9. Q.L. He and N. Standish, *ISIJ Int.* 30, 305 (1990).
10. T.M.J. Fabritius, P.T. Mure, and J.J. Härkki, *ISIJ Int.* 43, 1177 (2003).
11. T.M.J. Fabritius, P.T. Kurkinen, P.T. Mure, and J.J. Härkki, *Iron Steelmak* 32, 113 (2005).
12. H.J. Odenthal, U. Thiedemann, U. Falkenreck, and J. Schlueter, *Metall. Mater. Trans. B* 41, 396 (2010).
13. S.T. Johansen, J.Y. Wu, and W. Shyy, *Int. J. Heat Fluid Flow* 25, 10 (2004).
14. M.M. Li, L. Li, Q. Li, and Z.S. Zou, *JOM* 70, 2051 (2018).
15. C.W. Hirt and B.D. Nichols, *J. Comput. Phys.* 39, 981 (2011).
16. J.U. Brackbill, D.B. Kothe, and C. Zemach, *J. Comput. Phys.* 100, 335 (1992).
17. M. Sommerfield, *Numer. Methods Multiph. Flows ASME* 91, 11 (1990).
18. H.J. Odenthal, U. Falkenreck, and J. Schlüter, *ECCOMAS CFD* (TU: Delft, 2006).
19. B. Deo and R. Boom, *Fundamentals of Steelmaking Metallurgy* (Upper Saddle River: Prentice Hall, 1993).
20. FLUENT, *14.0 Manual* (Canonsburg: Ansys Inc, 2011).
21. E.O. Brigham, *The Fast Fourier Transform and Its Application* (Englewood Cliffs: Prentice Hall, 1940).
22. F. Oeters, *Metallurgy of Steelmaking* (Berlin: Springer-Verlag, 1997).